PHYSICAL REVIEW C **83**, 021304(R) (2011)

Dipole responses in Nd and Sm isotopes with shape transitions

Kenichi Yoshida and Takashi Nakatsukasa
RIKEN Nishina Center for Accelerator-Based Science, Wako, Saitama 351-0198, Japan
(Received 9 August 2010; revised manuscript received 24 January 2011; published 18 February 2011)

Photoabsorption cross sections of Nd and Sm isotopes from spherical to deformed even nuclei are systematically investigated by means of the quasiparticle-random-phase approximation based on the Hartree-Fock-Bogoliubov ground states using the Skyrme energy density functional. The gradual onset of deformation in the ground states as the neutron number increases leads to characteristic features of the shape phase transition. The calculations well reproduce the isotopic dependence of broadening and the emergence of a double-peak structure in the cross sections without any adjustable parameter. We also find that the deformation plays a significant role for low-energy dipole strengths. The $E1$ strengths are fragmented and considerably lowered in energy. The summed $E1$ strength up to 10 MeV is enhanced by a factor of 5 or more.

DOI: 10.1103/PhysRevC.83.021304 PACS number(s): 21.10.Re, 21.60.Jz, 24.30.Cz, 27.60.+j

Density functional theory has been widely used to describe a variety of quantum many-body systems [1] including nuclear many-body systems [2]. Recent advances in computing capability together with highly developed techniques in the nuclear energy-density-functional (EDF) method allow us to calculate the ground-state properties of nuclei in the entire mass region [3]. The nuclear ground-state deformation is one such property, which is an example of the spontaneous breaking of rotational symmetry. Experimental evidence of nuclear shape changes is related to low-lying quadrupole collectivity, such as the ratio of the excitation energies of 2^+ and 4^+ states, E_{4+}/E_{2+}, the reduced transition probability $B(E2; 2^+ \to 0^+)$, etc. However, it is known that the nuclear deformation also affects the high-frequency collective modes of excitation, giant resonances (GRs) [4,5]. For instance, peak splitting of the giant dipole resonance (GDR), which is caused by the different frequencies of oscillation along the long and short axes, has been observed in experiments [6]. A typical example of the shape phase transition from spherical to deformed ground states and the evolution of the deformation splitting in GDRs have been observed in Nd and Sm isotopes [4–8]. In this Rapid Communication, we report a first systematic calculation of electric dipole ($E1$) responses for these heavy isotopes at the shape phase transition, using a nonempirical approach with the Skyrme EDF, namely, the quasiparticle-random-phase-approximation (QRPA) based on the Hartree-Fock-Bogoliubov (HFB) ground states.

GDRs in heavy deformed systems have been previously investigated using the separable QRPA with the Skyrme EDF [9,10]. The separable approximation in the QRPA, perhaps, provides a good approximation for the GDR. It is, however, difficult to analyze the low-lying states because the structure of normal modes is nontrivial and significantly affected by the detailed shell structure. The low-energy $E1$ strengths, which are often discussed as the pygmy dipole resonance (PDR), have attracted considerable interest. A nonstatistical distribution of the $E1$ strengths close to the threshold has a strong impact on the astrophysical r-process nucleosynthesis [11]. In addition, the PDR is a typical example of exotic collective modes expected in neutron-rich nuclei and has been extensively studied with the EDF approaches [12]. However, the effect of deformation on the PDR has been studied only for light nuclei [13,14], except for a recent study on Sn isotopes with the relativistic EDF [15].

We have developed a new parallelized computer code of the HFB + QRPA, which is an extended version of that developed in Ref. [16], to add the residual spin-orbit interaction. The residual Coulomb interaction is neglected because of computational limitations. We expect that the residual Coulomb plays only a minor role [14,17,18]. In Ref. [18], the effects of neglecting the residual Coulomb interaction are discussed in detail: The centroid energy of the GDR can be shifted by about 400 keV at maximum. However, this amount of change does not affect the discussion in the present paper.

To describe the nuclear deformation and the pairing correlations, simultaneously, with a good account of the continuum, we solve the HFB equations [19] in the coordinate space using cylindrical coordinates $\mathbf{r} = (\rho, z, \phi)$ with a mesh size of $\Delta\rho = \Delta z = 0.6$ fm and a box boundary condition at $(\rho_{\max}, z_{\max}) = (14.7, 14.4)$ fm. We assume axial and reflection symmetries in the ground state. The differential operators are represented by use of the 11-point formula of the finite-difference method. Since the parity (π) and the magnetic quantum number (Ω) are good quantum numbers, the HFB Hamiltonian is in a block diagonal form with respect to each (Ω^π, q) sector, where q stands for a neutron or proton. The HFB equations for each sector are solved independently with 48 processors for the quasiparticle (qp) states up to $\Omega = 23/2$ with positive and negative parities. Then, the densities and HFB Hamiltonian are updated, which requires communication among the 48 processors. A modified Broyden method [20] is utilized to calculate new densities. The qp states are truncated according to the qp energy cutoff at $E_\alpha \leqslant 60$ MeV.

We introduce an additional truncation for the QRPA calculation, in terms of the two-quasiparticle (2qp) energy, as $E_\alpha + E_\beta \leqslant 60$ MeV. This reduces the number of 2qp states to, for instance, about 38 000 for the $K^\pi = 0^-$ excitation in ^{154}Sm. The calculation of the QRPA matrix elements in the qp basis is performed on the parallel computers. In the present calculation, all the matrix elements are real and we use 512 processors to compute them. To save computing time for diagonalization of the QRPA matrix, we employ a technique to reduce the generalized eigenvalue problems to the diagonalization

of a real symmetric matrix of half the dimension [21,22]. For diagonalization of the matrix, we use the SCALAPACK PDSYEV subroutine [23]. To calculate the QRPA matrix elements and to diagonalize the matrix, it takes about 390 and 135 CPU hours, respectively. Similar calculations using the HFB + QRPA for axially deformed nuclei have recently been reported [15,22,24,25]. In particular, the QRPA calculation by Terasaki and Engel in Ref. [25] is analogous to ours. They adopt the canonical-basis representation and introduce a further truncation according to the occupation probabilities of 2qp excitations. In contrast, we adopt the qp representation and a truncation simply owing to the 2qp energies.

For the normal (particle-hole) part of the EDF, we employ the SkM* functional [26]. For the pairing energy, we adopt the one in Ref. [27], which depends on both the isoscalar and isovector densities, in addition to the pairing density, with the parameters given in Table III of Ref. [27].

Since the full self-consistency between the static mean-field calculation and the dynamical calculation is slightly broken by the neglected residual terms and the truncation of the 2qp states, spurious states may appear at finite excitation energies. In the present calculation, the excitation energies of the spurious states with $K^\pi = 0^-$ and 1^-, corresponding to the center-of-mass motion, become imaginary in ^{154}Sm, $1.46i$ and $1.60i$ MeV, respectively. A small contamination by the spurious component does not affect the GDRs because they are far apart in energy. We have also confirmed that, using the method in Ref. [14], the residual Coulomb interaction does not lead to a sizable difference in the dipole strength functions. To remove the small spurious component of the center-of-mass motion from the physical excitations, we employ the procedure in Ref. [28].

Figure 1 shows the ground-state deformation of Nd and Sm isotopes obtained with the HFB calculation. The calculated intrinsic electric quadrupole moments are compared with the experimental values [29]. The calculation well reproduces the evolution of quadrupole deformation for $N \geqslant 86$. For spherical nuclei with $N = 82$ and 84, we also plot the values deduced from $B(E2; 0^+ \to 2^+)$ obtained by the QRPA calculation. The collectivity of the 2^+ state is apparently overestimated at $N = 84$, because these nuclei are so soft with respect to the quadrupole deformation that the QRPA cannot describe the 2^+ state properly.

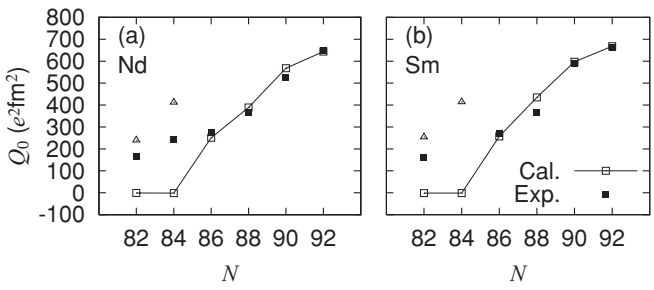

FIG. 1. Intrinsic electric quadrupole moments of Nd and Sm isotopes. For spherical nuclei, values extracted from calculated $B(E2)$ are shown by triangles. The experimental values are taken from Ref. [29].

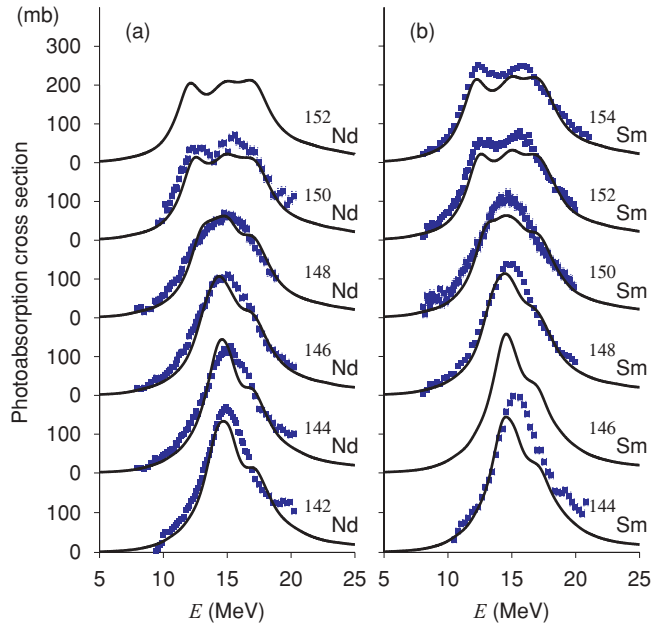

FIG. 2. (Color online) Photoabsorption cross sections in (a) Nd and (b) Sm isotopes as functions of photon energy. The experimental data [7,8] are denoted by filled squares.

Based on these HFB ground states, we perform the QRPA calculation to obtain the excitation energies $\hbar\omega_i$ and the transition matrix elements $\langle i|\hat{F}^1_{1K}|0\rangle$. The photoabsorption cross section is calculated as

$$\sigma_{\rm abs}(E) = \frac{4\pi^2 E}{\hbar c} \sum_{K=-1}^{1} \frac{dB\left(E, F^1_{1K}\right)}{dE}, \tag{1}$$

$$\frac{dB(E, F^1_{1K})}{dE} = \frac{2E\gamma}{\pi} \sum_i \frac{\tilde{E}_i \left|\langle i|\hat{F}^1_{1K}|0\rangle\right|^2}{\left(E^2 - \tilde{E}_i^2\right)^2 + E^2\gamma^2}, \tag{2}$$

where $\tilde{E}_i^2 = (\hbar\omega_i)^2 + \gamma^2/4$ [4]. The smearing width γ is set to 2 MeV, which is supposed to simulate the spreading effect $\Gamma^\downarrow$ missing in the QRPA. The electric dipole operator $\hat{F}^1_{1K}$ is defined in Eq. (6-175) of Ref. [4].

We show in Fig. 2 the calculated photoabsorption cross sections in the GDR energy region together with the available experimental data [7,8]. The GDR peak energies agree well with the experimental values and produce the deformation splitting in ^{150,152}Nd and ^{152,154}Sm. Previously, separable QRPA calculations with SkM* [9,10] produced a significantly larger second peak for these deformed nuclei, which disagrees with the experiment. This peak is diminished in the present full QRPA calculation. The GDR width calculated with $\gamma =$ 2 MeV is also in good accordance with the experimental values. The QRPA accounts for the Landau damping, which is a fragmentation of the GDR strength into nearby 2qp states, but not for the spreading effect, which corresponds to a fragmentation into more complex states. The nice agreement on the broadening indicates that the smearing width $\gamma =$ 2 MeV has a good correspondence with the spreading width $\Gamma^\downarrow$ in these nuclei.

The isotopic dependence of the peak broadening is well reproduced, surprisingly, even for the transitional nuclei. The

width for $N = 82$ and 84 is calculated as $\Gamma \approx 4.5$ MeV, and it gradually increases to about 6 MeV for $N = 88$; then the splitting becomes visible for $N \geqslant 90$. Here, the width Γ is evaluated by fitting the calculated cross section with a Lorentz line. This broadening effect is commonly interpreted as mode-mode coupling effects with the low-lying collective modes [5]. In the present QRPA calculation, the mode coupling is not explicitly taken into account. However, the QRPA based on the deformed HFB state may implicitly include a part of the coupling effect. Figure 2 shows that the isotopic dependence can be well accounted for by a gradual increase of the ground-state deformation. However, the small increase of the width from ^{142}Nd to ^{144}Nd observed in the experiment cannot be fully reproduced in the calculation. Since the HFB calculation produces a spherical ground state for ^{144}Nd, this requires an explicit higher-order calculation beyond the QRPA.

We may notice another small disagreement in the peak shape: The calculated GDR peak has a shoulder in the spherical nuclei, and this shoulder becomes a third peak in the deformed nuclei. This is due to the Landau fragmentation; however, this feature is not clearly observed in experiments. As discussed in the following, the detailed properties of the Landau fragmentation depend on the choice of the Skyrme EDF. For instance, the fragmentation effect becomes weaker with the SkP functional, giving a better agreement with the experiments.

Figure 3 shows photoabsorption cross sections in ^{144,154}Sm obtained by employing the SLy4 [30] and SkP [19] functionals. In all the calculations, the energy-weighted strengths summed up to 60 MeV agree with the calculated sum-rule values within 3% accuracy. However, the magnitude of the enhancement factor (κ) depends on the parameter set: $\kappa = 0.39$, 0.18, and 0.25 in the SkM*, SLy4 and SkP functionals, respectively, for the Sm isotopes under investigation.

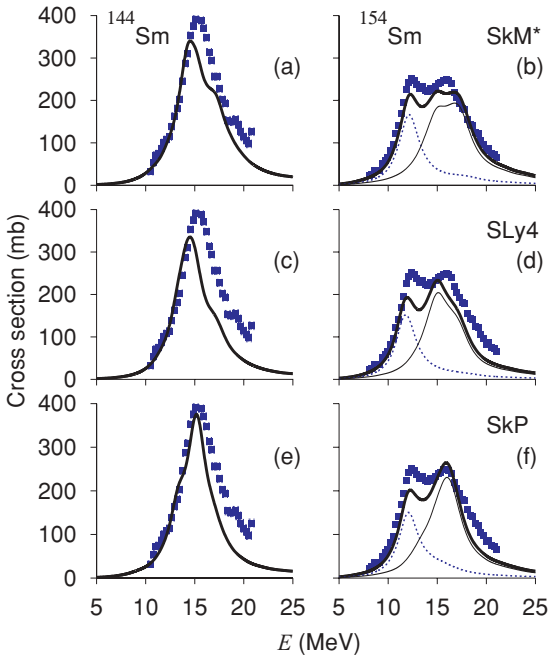

FIG. 3. (Color online) Photoabsorption cross sections of ^{144}Sm and ^{154}Sm obtained by employing the SkM*, SLy4, and SkP functionals. The $K^\pi = 0^-$ and $K^\pi = 1^-$ components are shown by dotted and thin solid lines, respectively, in ^{154}Sm.

The experimental GDR peak structure is reproduced not only by using the SkM* functional but also by employing other commonly used Skyrme functionals, though the SLy4 functional gives slightly smaller GDR peak energies and smaller summed strengths. The SkP reproduces the energy and the shape best among the three functionals. For spherical nuclei, the cross section obtained with the SkP functional can be nicely fitted by a single Lorentzian curve. For deformed nuclei, the lower ($K = 0$) peak shows a Lorentz shape for any of the functionals, while the upper ($K = 1$) peak shows visible distortion for SkM* and SLy4. This difference may be due to different properties of the Landau fragmentation because the 2qp states in the background are more widely spread in energy with a smaller effective mass. Actually, the effective mass is largest ($m^*/m \approx 1$) in SkP.

Next, we discuss the low-energy $E1$ strengths. Photon scattering experiments at Technische Universität Darmstadt [31] reported the 1^- states up to 9.9 MeV and found the concentration of the dipole strength in $N = 82$ semimagic nuclei at energies between 5.5 and 8 MeV. Figures 4 and 5 show the $E1$ strengths below 10 MeV calculated with the SkM* functional. The SLy4 and SkP functionals provide very similar results. In the spherical ^{142}Nd and ^{144}Sm nuclei, we can see a concentration of the dipole strength between 8 and 10 MeV. The same concentration can be seen in the unperturbed strength distribution, which may suggest a weak collectivity. Apparently, the calculated strength distribution is too high in energy. Similar disagreements have also been observed in a relativistic QRPA calculation [32]. However, the $B(E1\uparrow)$ value summed up to 10 MeV in ^{144}Sm is 0.27 e^2 fm^2, which agrees reasonably well with the experimental value 0.20 e^2 fm^2. This seems to suggest that these low-energy $E1$ strengths are redistributed to two-phonon ($2^+ \otimes 3^-$) and multiphonon states, which are located at energies 3–7 MeV, by higher-order coupling effects [31].

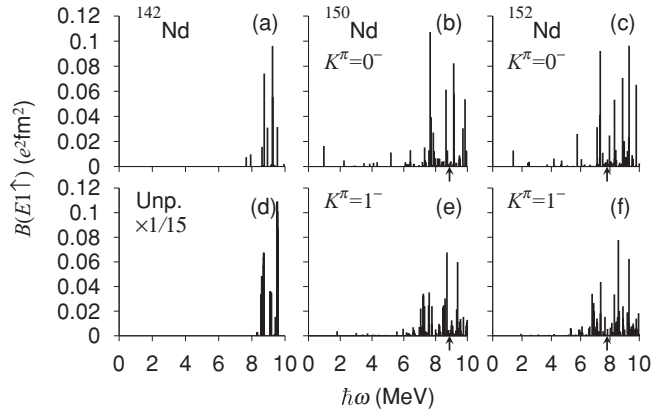

FIG. 4. Calculated low-energy $E1$ strengths $B(E1; 0^+ \rightarrow 1^-)$ as functions of energy in ^{142,150,152}Nd. The arrow indicates the neutron emission threshold energy. (d) shows the unperturbed strengths multiplied by 1/15 in ^{142}Nd. The neutron threshold of ^{142}Nd is 11.6 MeV.

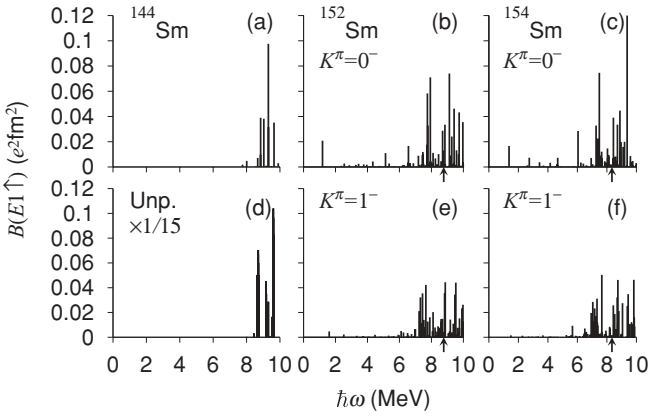

FIG. 5. As Fig. 4 but in ^{144,152,154}Sm. (d) shows the unperturbed strengths multiplied by $1/15$ in ^{144}Sm. The neutron threshold of ^{144}Sm is 11.9 MeV.

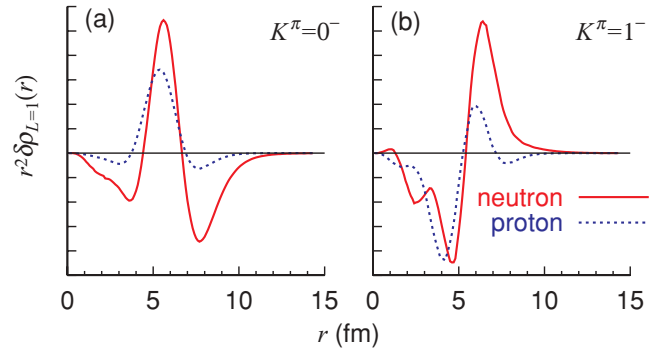

FIG. 6. (Color online) Calculated transition densities of the $K^\pi = 0^-$ state at 7.49 MeV and of the $K^\pi = 1^-$ state at 7.33 MeV in ^{154}Sm.

It is quite challenging to describe such multiphonon states on the basis of the nuclear EDF method [33,34]; however, it is beyond the scope of the present analysis.

In contrast to the spherical nuclei, the deformed nuclei show significant fragmentation of the $E1$ strength into low-energy states. For ^{150,152}Nd and ^{152,154}Sm, the calculated energies of the lowest $K^\pi = 0^-$ states are 0.97, 1.40, 1.10, and 1.37 MeV, and those of $K^\pi = 1^-$ states are 1.80, 1.93, 1.60, and 1.49 MeV. These values agree well with available experimental values for octupole vibrational states [35]. The deformation significantly increases the total low-energy $E1$ strength. Actually, the summed strengths up to 10 MeV, $\sum B(E1\uparrow) \approx 1.5\ e^2$ fm^2, are about five times larger than those of spherical nuclei. It may be of significant interest to study how this low-energy $E1$ enhancement caused by deformation affects the element synthesis scenario. In the deformed nuclei, ^{150,152}Nd and ^{152,154}Sm, there are no experimental data available for the low-lying strengths below the neutron-emission threshold energy. It would thus be interesting to investigate experimentally the low-lying dipole strengths in these nuclei.

The conclusion of the present calculation on the effect of deformation is opposite to that reached in the study of Sn isotopes in Ref. [15]. Those authors showed that the low-lying $E1$ strength is smaller in deformed nuclei than in spherical nuclei. To clarify the origin of this difference, we need to examine several possible effects: First, the effect of neutron excess should be investigated. From the technical point of view, the two calculations use different treatments for the pairing. We adopt the Bogoliubov method and the authors of Ref. [15] use the BCS approximation. The treatment of continuum and weakly bound orbitals is also different: The wave functions are expanded in the harmonic oscillator basis in Ref. [15], while they are directly expressed in the coordinate space in the present study. The calculations of Ref. [15] are fully self-consistent, and they do not have the contamination of the spurious center-of-mass motion in the physical excitations. We should, therefore, investigate the roles of deformation, neutron excess, pairing, and the continuum in the low-lying strengths in various isotopic chains, paying attention to the mixing of spurious components, as a future work.

We also confirm that the dipole states around 7 MeV have a character different from the GDR. In Fig. 6, the transition densities, approximately projected to the laboratory frame [36], are shown on arbitrary scales. These dipole states predominantly have an isoscalar character: The proton and neutron transition densities have the same sign. Neutron dominance can be seen at $r > 7$ fm; however, the proton contribution does not completely vanish. These characters of the PDR are consistent with the previous QRPA analysis for spherical nuclei of $N = 82$ isotones [32]. As the N/Z ratio increases away from stability, we expect that the neutron-dominant character will develop in the surface region.

In summary, we have investigated effects of the shape transition on the $E1$ strength distribution in rare-earth nuclei, using the newly developed parallelized HFB + QRPA calculation code with the Skyrme EDF. This enables us to simultaneously study both high-energy GRs and low-energy collective and noncollective states. The typical characteristics of the GDR in the shape phase transition from spherical to deformed nuclei, especially the isotopic dependence of the broadening and splitting of the GDRs, are extremely well reproduced in the calculation. We have also found that the deformation plays a significant role in the low-energy $E1$ strength distribution: The $E1$ strength is distributed to low-energy states and the total strength at $E < 10$ MeV is roughly five times enhanced, compared to the spherical nuclei. The low-energy strengths in spherical ^{144}Sm as calculated are too high in energy. Inclusion of the higher-order mode-mode coupling is desirable for further improvements. Systematic calculations with the HFB + QRPA for spherical-to-deformed and light-to-heavy nuclei help us not only to understand and to predict new types of collective modes of excitation, but also to shed light on the nuclear EDF of new generations.

One of the authors (K.Y.) is supported by the Special Postdoctoral Researcher Program of RIKEN. The work is supported by Grants-in-Aid for Scientific Research (Nos. 21340073 and 20105003) and by the Joint Research Program at the Center for Computational Sciences, University of Tsukuba. The numerical calculations were performed on the RIKEN Integrated Cluster of Clusters (RICC).

[1] R. G. Parr, Annu. Rev. Phys. Chem. **34**, 631 (1983).
[2] M. Bender, P-H. Heenen, and P-G. Reinhar, Rev. Mod. Phys. **75**, 121 (2003).
[3] M. V. Stoitsov, J. Dobaczewski, W. Nazarewicz, S. Pittel, and D. J. Dean, Phys. Rev. C **68**, 054312 (2003).
[4] A. Bohr and B. R. Motteleson, *Nuclear Structure* (Benjamin, New York, 1975; World Scientific, Singapore, 1998), Vol. II.
[5] M. N. Harakeh and A. van der Wounde, *Giant Resonances* (Oxford University Press, Oxford, 2001).
[6] B. L. Berman and S. C. Fultz, Rev. Mod. Phys. **47**, 713 (1975).
[7] P. Carlos, H. Beil, R. Bergere, A. Lepretre, and A. Veyssiere, Nucl. Phys. A **172**, 437 (1971).
[8] P. Carlos, H. Beil, R. Bergère, A. Leprêtre, A. De Miniac, and A. Veyssière, Nucl. Phys. A **225**, 171 (1974).
[9] V. O. Nesterenko, W. Kleinig, J. Kvasil, P. Vesely, P.-G. Reinhard, and D. S. Dolci, Phys. Rev. C **74**, 064306 (2006).
[10] V. O. Nesterenko, W. Kleinig, J. Kvasil, P. Vesely, and P.-G. Reinhard, Int. J. Mod. Phys. E **17**, 89 (2008).
[11] S. Goriely and E. Khan, Nucl. Phys. A **706**, 217 (2002).
[12] N. Paar, D. Vretenar, E. Khan, and G. Colò, Rep. Prog. Phys. **70**, 691 (2007).
[13] K. Yoshida, Phys. Rev. C **80**, 044324 (2009).
[14] S. Ebata, T. Nakatsukasa, T. Inakura, K. Yoshida, Y. Hashimoto, and K. Yabana, Phys. Rev. C **82**, 034306 (2010).
[15] D. Pena Arteaga, E. Khan, and P. Ring, Phys. Rev. C **79**, 034311 (2009).
[16] K. Yoshida and N. V. Giai, Phys. Rev. C **78**, 064316 (2008).
[17] J. Terasaki, J. Engel, M. Bender, J. Dobaczewski, W. Nazarewicz, and M. Stoitsov, Phys. Rev. C **71**, 034310 (2005).
[18] Tapas Sil, S. Shlomo, B. K. Agrawal, and P. G. Reinhard, Phys. Rev. C **73**, 034316 (2006).
[19] J. Dobaczewski, H. Flocard, and J. Treiner, Nucl. Phys. A **422**, 103 (1984).
[20] A. Baran, A. Bulgac, M. M. Forbes, G. Hagen, W. Nazarewicz, N. Schunck, and M. V. Stoitsov, Phys. Rev. C **78**, 014318 (2008).
[21] P. Ring and P. Schuck, *The Nuclear Many-Body Problem* (Springer, Berlin, 1980).
[22] S. Péru and H. Goutte, Phys. Rev. C **77**, 044313 (2008).
[23] [http://www.netlib.org/scalapack/].
[24] C. Losa, A. Pastore, T. Døssing, E. Vigezzi, and R. A. Broglia, Phys. Rev. C **81**, 064307 (2010).
[25] J. Terasaki and J. Engel, Phys. Rev. C **82**, 034326 (2010).
[26] J. Bartel, P. Quentin, M. Brack, C. Guet, and H.-B. Håkansson, Nucl. Phys. A **386**, 79 (1982).
[27] M. Yamagami, Y. R. Shimizu, and T. Nakatsukasa, Phys. Rev. C **80**, 064301 (2009).
[28] K. Yoshida, Eur. Phys. J. A **42**, 583 (2009).
[29] [http://ie.lbl.gov/ensdf/].
[30] E. Chabanat, P. Bonche, P. Haensel, J. Meyer, and R. Schaeffer, Nucl. Phys. A **627**, 710 (1997).
[31] A. Zilges, S. Volz, M. Babilon, T. Hartmann, P. Mohr, and K. Vogt, Phys. Lett. B **542**, 43 (2002).
[32] N. Paar, P. Ring, T. Nikšić, and D. Vretenar, Phys. Rev. C **67**, 034312 (2003).
[33] D. Sarchi, P. F. Bortignon, and G. Colò, Phys. Lett. B **601**, 27 (2004).
[34] E. Litvinova, P. Ring, and V. Tselyaev, Phys. Rev. Lett. **105**, 022502 (2010).
[35] P. C. Sood, D. M. Headly, and R. K. Sheline, At. Data Nucl. Data Tables **47**, 89 (1991).
[36] D. Peña Arteaga and P. Ring, Phys. Rev. C **77**, 034317 (2008).